International Journal of Radiation Oncology biology • physics

www.redjournal.org

Physics Contribution

Clinical Implementation of Dual-energy CT for Proton Treatment Planning on Pseudo-monoenergetic CT scans

Patrick Wohlfahrt, MSc,[*,†] Christian Möhler, MSc,[‡,§] Volker Hietschold, PhD,[*,||] Stefan Menkel, PhD,[¶] Steffen Greilich, PhD,[‡,§] Mechthild Krause, MD, PhD,[*,†,¶,#,] Michael Baumann, MD, PhD,[*,†,¶,#,**] Wolfgang Enghardt, PhD,[*,†,¶,#] and Christian Richter, PhD[*,†,¶,#]**

OncoRay - National Center for Radiation Research in Oncology, Faculty of Medicine and University Hospital Carl Gustav Carus, Technische Universität Dresden, Helmholtz-Zentrum Dresden - Rossendorf; [†]Helmholtz-Zentrum Dresden - Rossendorf, Institute of Radiooncology, Dresden; [‡]German Cancer Research Center; [§]National Center for Radiation Research in Oncology, Heidelberg Institute for Radiation Oncology, Heidelberg; Departments of [||]Diagnostic Radiology and [¶]Radiation Oncology, Faculty of Medicine and University Hospital Carl Gustav Carus, Technische Universität Dresden; [#]German Cancer Consortium; and **National Center for Tumor Diseases, Dresden, Germany

Received Jun 15, 2016, and in revised form Oct 11, 2016. Accepted for publication Oct 14, 2016.

Summary

To clinically exploit the physical advantages of protons, a precise prediction of proton range from computed tomography (CT) is required. Dual-energy CT (DECT) can contribute to reduce CT-related uncertainties and thus minimize the irradiation of normal tissue. However,

Purpose: To determine whether a standardized clinical application of dual-energy computed tomography (DECT) for proton treatment planning based on pseudomonoenergetic CT scans (MonoCTs) is feasible and increases the precision of proton therapy in comparison with single-energy CT (SECT).

Methods and Materials: To define an optimized DECT protocol, CT scan settings were analyzed experimentally concerning beam hardening, image quality, and influence on the heuristic conversion of CT numbers into stopping-power ratios (SPRs) and were compared with SECT scans with identical CT dose. Differences in range prediction and dose distribution between SECT and MonoCT were quantified for phantoms and a patient.

Results: Dose distributions planned on SECT and MonoCT datasets revealed mean range deviations of 0.3 mm, γ passing rates (1%, 1 mm) greater than 99.9%, and

Reprint requests to: Patrick Wohlfahrt, MSc, OncoRay - National Center for Radiation Research in Oncology, Faculty of Medicine and University Hospital Carl Gustav Carus, Technische Universität Dresden, Helmholtz-Zentrum Dresden - Rossendorf, Dresden, Germany. Tel: (+49) 351-458-7626; E-mail: Patrick.Wohlfahrt@OncoRay.de

Supported in part by the National Center for Radiation Oncology within the project "translation of dual-energy CT into application in particle therapy". CR is funded by the German Federal Ministry for Education and Research (Grant No. BMBF-03Z1N51).

Conflict of interest: none.

Supplementary material for this article can be found at www.redjournal.org.

Acknowledgment—The authors thank Gert Rothe of the Department of Radiation Oncology, Faculty of Medicine and University Hospital Carl Gustav Carus, Technische Universität Dresden, for producing all the noncommercial phantoms used in this study.

Int J Radiation Oncol Biol Phys, Vol. 97, No. 2, pp. 427–434, 2017

http://dx.doi.org/10.1016/j.ijrobp.2016.10.022

voxelwise DECT-based approaches are not yet clinically validated. Hence, a stepwise clinical implementation of DECT using pseudo-monoenergetic CT images is proposed, evaluated on phantom and patient datasets, and finally routinely introduced in proton therapy.

no clinically relevant changes in dose-volume histograms. However, image noise and CT-related uncertainties could be reduced by MonoCT compared with SECT, which resulted in a slightly decreased dependence of SPR prediction on beam hardening. Consequently, DECT was clinically implemented at the University Proton Therapy Dresden in 2015. Until October 2016, 150 patients were treated based on MonoCTs, and more than 950 DECT scans of 351 patients were acquired during radiation therapy.

Conclusions: A standardized clinical use of MonoCT for treatment planning is feasible, leads to improved image quality and SPR prediction, extends diagnostic variety, and enables a stepwise clinical implementation of DECT toward a physics-based, patient-specific, nonheuristic SPR determination. Further reductions of CT-related uncertainties, as expected from such SPR approaches, can be evaluated on the resulting DECT patient database.

Introduction

The physical benefit of proton therapy compared with photon therapy can contribute to high tumor coverage while sparing normal tissue more effectively (1-3). To improve the clinical exploitation of theoretic advantages, current uncertainties in proton range prediction from computed tomography (CT) have to be further minimized (4, 5). Inasmuch as proton treatment planning today is based on single-energy CT (SECT), CT-related uncertainties and the heuristic conversion of CT numbers into stopping-power ratios (SPRs) using a universal Hounsfield look-up table (HLUT) limit treatment accuracy. Additional margins of about 3.5% of absolute range are clinically used in beam direction to take account of these uncertainties. It has been shown that dual-energy CT (DECT) can potentially contribute to more precise proton range predictions (6-11). However, current findings are mainly based on DECT scans of homogeneous tissue substitutes and simplified inhomogeneous phantoms, which were tested retrospectively on a few DECT scans of head trauma patients (11) acquired with nonoptimized DECT protocols for radiation therapy. Although voxelwise DECT-based SPR prediction approaches are subject to intensive research activities (8, 12), they are not yet clinically validated and applied because several challenges, for example, integration into commercial treatment planning systems (TPS), are still to be solved. Hence, a stepwise clinical implementation of DECT is highly advisable if not even inevitable. We propose here an approach, starting with treatment planning on DECT-based pseudo-monoenergetic CT datasets (MonoCTs) still using a heuristic CT-number-to-SPR conversion to ensure TPS compatibility and range prediction similar to SECT. For this purpose and in strict accordance with as low as reasonably achievable (ALARA) principles, the patient's SECT scan should be replaced by a DECT scan of similar or less CT dose. The DECT information can be used to calculate MonoCTs, which are an energy-dependent weighted sum of both single DECT scans acquired with 80/140 kVp (13):

$$H(E_{\text{mono}}) = \alpha(E_{\text{mono}})\, H_{80\text{kVp}} + [1 - \alpha(E_{\text{mono}})]\, H_{140\text{kVp}} \quad (1)$$

To guarantee the clinical feasibility and safety of proton treatment planning on MonoCTs instead of SECT scans, specific requirements have to be fulfilled, which were evaluated within this study: similar image quality, at least comparable precision in range prediction, and no clinically relevant changes in dose distributions. This stepwise clinical implementation already provides with MonoCTs more possibilities to increase tissue contrast (14-18) and to reduce metal artifacts (13, 19), and it offers the opportunity to determine the ultimate role of DECT in proton therapy in a subsequent step by quantifying the potential benefits of a patient-specific DECT-based proton range prediction on a large DECT tumor patient database.

Methods and Materials

CT measurements for DECT scan protocol optimization

To determine the optimized MonoCT energy E_{mono} for treatment planning with regard to beam hardening and image quality, 17 cylindrical material samples (25 mm diameter, 10 mm length) distributed over the CT number scale from −1024 to 3071 HU were investigated. These samples were aligned in series along the central scanner axis of a single-source CT scanner Siemens Somatom Definition AS (Siemens Healthineers, Forchheim, Germany) and scanned in 3 setups simulating different beam hardening conditions: without additional phantom material (referred to as Air), in a water reservoir (Water), and in the water reservoir with

additional lateral cortical bone substitutes (Pelvis). More detailed information is provided in Supplement EA (available online at www.redjournal.org).

The CT images were acquired in single-energy (SE) and dual-energy (DE) modes with identical CT dose and scan settings optimized with respect to beam hardening and image quality (Table 1). The 2 CT scans in DE mode were acquired sequentially with a delay of approximately 10 to 15 seconds depending on scan regions.

For each investigated material i, its scan-specific CT number H_i and corresponding standard deviation σ_i were determined in regions of interest with 18 mm diameter. To obtain x-ray attenuation properties in humans, CT numbers of 71 tabulated human tissues (20, 21) were calculated with an in-house optimized scanner-specific stoichiometric CT number prediction (22, 23), which was calibrated based on the elemental composition and measured CT number of the scanned tissue substitutes.

CT number prediction of MonoCT datasets

The DECT applications Monoenergetic imaging (Mono) and syngo.CT DE Monoenergetic Plus (MonoPlus) of the imaging software syngo.via (Siemens Healthineers) were used to convert the DECT datasets into MonoCTs of 29 energies ranging from 40 to 190 keV. MonoPlus is a further development of Mono including an integrated multiband filter (not applicable to SECT) for improved noise suppression (14, 24, 25). Both applications use deformable image registration by default to ensure voxelwise computations based on sequentially acquired DECT scans.

For both DECT implementations, the energy-dependent pseudo-monoenergetic CT number H_i (E_{mono}) was determined for the 17 scanned materials and 71 tabulated human tissues in the 3 scan setups as described above. The standard deviation σ_i (E_{mono}) of H_i (E_{mono}) was additionally calculated for the scanned samples.

Moreover, it was checked whether the pseudo-monoenergetic CT numbers obtained by Mono or MonoPlus for a specific energy (and material) matched the CT numbers corresponding to the monoenergetic X-rays of the same energy. Therefore, monoenergetic CT numbers (MonoNIST) were calculated based on material-specific photon cross-sections (26). According to equation 1, the energy-dependent weighting factor α was computed for Mono, MonoPlus, and MonoNIST.

Table 1 Computed tomography (CT) scan protocols

CT scan parameter	Single-energy CT (SECT)	Dual-energy CT (DECT)	
Tube voltage/kV	120	80	140
Current time product/mAs	258	400	95
$\mathrm{CTDIvol}_{32\mathrm{cm}}$/mGy	20.8	9.6	11.1
Acquisition	24 × 1.2 mm	24 × 1.2 mm	
Reconstruction kernel	D34	D34	

More detailed information is presented in Supplement EB (available online at www.redjournal.org).

Image parameters for quantitative MonoCT evaluation

To evaluate the image noise and beam hardening effects on CT numbers of MonoCT datasets compared with 120 kVp SECT scans (current clinical standard), the energy-dependent image-noise ratio (INR):

$$\mathrm{INR}(E_{\mathrm{mono}}) = \sqrt{\frac{1}{n}\sum_{i=1}^{n}\frac{\sum_{s\in\mathscr{S}}\sigma^2_{120\mathrm{kVp},\,s,\,i}}{\sum_{s\in\mathscr{S}}\sigma^2_{s,\,i}(E_{\mathrm{mono}})}} \tag{2}$$

and beam-hardening ratio (BHR):

$$\mathrm{BHR}(E_{\mathrm{mono}}) = \frac{\sum_i^n\left(\max\limits_{s\in\mathscr{S}}\{H_{120\mathrm{kVp},\,s,\,i}\} - \min\limits_{s\in\mathscr{S}}\{H_{120\mathrm{kVp},\,s,\,i}\}\right)}{\sum_i^n\left(\max\limits_{s\in\mathscr{S}}\{H_{s,\,i}(E_{\mathrm{mono}})\} - \min\limits_{s\in\mathscr{S}}\{H_{s,\,i}(E_{\mathrm{mono}})\}\right)} \tag{3}$$

with scan setups $\mathscr{S}=\{\mathrm{Air},\ \mathrm{Water},\ \mathrm{Pelvis}\}$ are introduced, respectively. Both quantities were determined for 29 energies E_{mono} using Mono and MonoPlus. All n tissue substitutes (except lung substitutes for INR because of material inhomogeneity) were included in this analysis ($n=9$ for INR, $n=11$ for BHR).

Heuristic CT-number-to-SPR conversion

For proton SPR prediction on CT images, an HLUT was defined by CT scans (Water setup) and relative range measurements with 125 MeV protons as described in (27). The CT numbers were determined for cylindrical materials with a diameter of 10 mm and SPRs for the same materials with a diameter of 50 mm. The SPRs of the tabulated human tissues were calculated using the Bethe formula with element-specific mean excitation energies (28) and Bragg's additivity rule (29).

To define the HLUT, the Hounsfield scale was divided into 3 parts representing different tissue types: low-density materials ($H < -150$ HU), soft tissues (-150 HU $\leq H \leq$ 150 HU), and bony tissues ($H >$ 150 HU). Each CT number segment was described by a linear function using only tissue substitutes. To avoid steps between adjacent linear functions, the intersection of both functions was set as transition point.

Evaluation of range prediction and dose calculation

To assess the influence of CT number variations between different beam hardening conditions (eg, different body regions) on the predicted proton range, these CT numbers were translated into SPRs using the HLUT previously

defined, and the mean and maximal range deviation between SECT and DECT were determined for a depth of 15 cm.

Moreover, SECT and DECT scans (Table 1) of a head phantom (PBU-60, Kyoto Kagaku, Kyoto, Japan) were evaluated concerning their influence on proton range calculation to verify consistent results and to ensure safe application of the new approach. Proton treatment planning in double-scattering mode was performed with XIO (Elekta AB, Stockholm, Sweden) using a $1 \times 1 \times 1$ mm^3 dose calculation grid and a beam traversing considerable tissue inhomogeneities until the distal edge of the target volume was reached. The treatment plan was optimized on the 120 kVp SECT scan and recalculated on MonoCTs. Deviations in range prediction were analyzed with line-dose profiles in beam direction and quantified by absolute range differences at 2 specific points: distal range at 90% (R_{90}) and 80% (R_{80}) of prescribed dose. Dose distributions were compared using a 2-dimensional γ analysis with a passing criteria of 1% dose difference and 1 mm distance to agreement (30) for all transverse CT slices receiving the prescribed dose.

Furthermore, to exclude possible differences between proton range prediction based on CT scans of a real human anatomy or a phantom consisting of tissue substitutes, the same analysis as described above was done for a patient with sacral chordoma for whom medically indicated SECT and DECT scans in direct succession were obtained. The clinically applied passively scattered proton treatment plan with 2 beams from 150° and 210° was evaluated. This retrospective analysis was approved by the local ethics committee (EK535122015).

Results

Evaluation of MonoCT image quality

The energy-dependent INR and BHR of Mono and MonoPlus are illustrated in Figure 1. For all energies, Mono shows an INR < 1 with a maximum at 70 keV. Consequently, for all MonoCT energies, the Mono algorithm leads to increased image noise in comparison with 120 kVp SECT scans with identical CT dose. Because of additional multiband filtering in MonoPlus, image noise can be clearly reduced in comparison with Mono. Especially for low and high energies, MonoPlus leads to a raised INR in comparison with Mono by up to 25% and

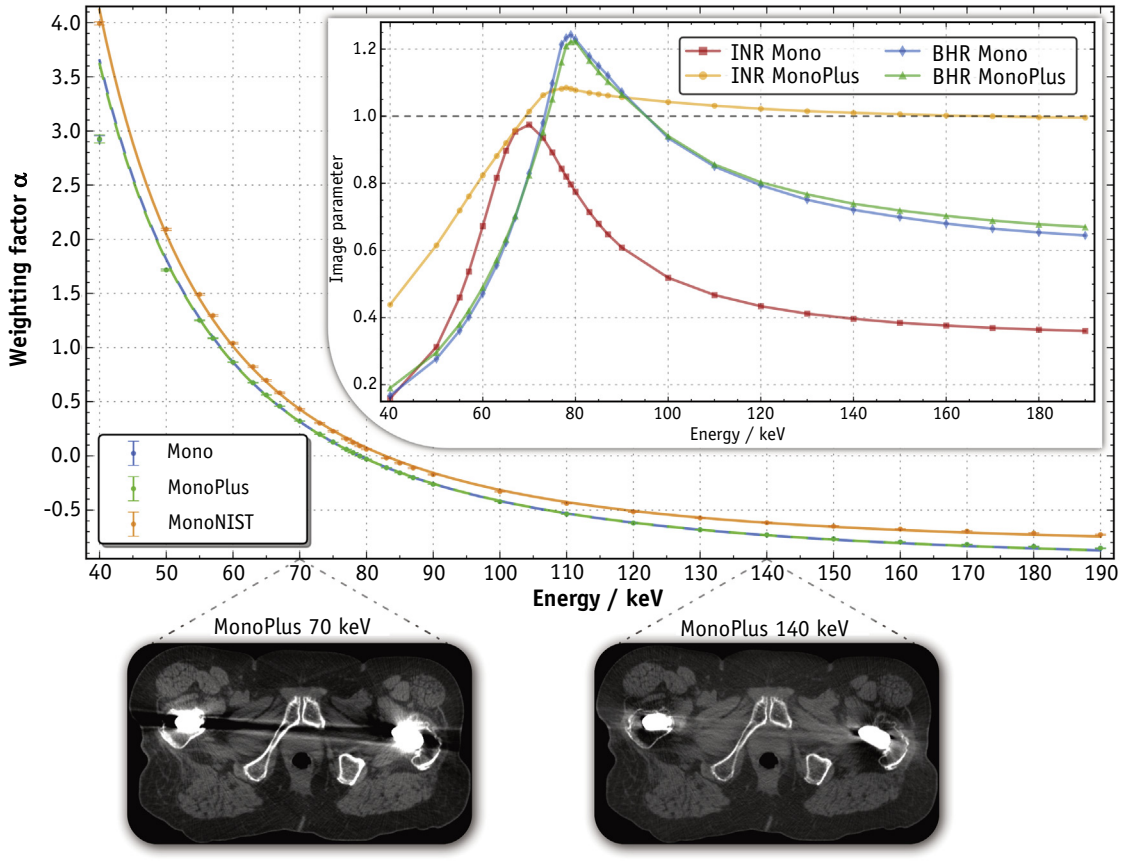

Fig. 1. Weighting factor α for MonoCT calculation, image-noise ratio (INR, inset), beam-hardening ratio (BHR, inset), and metal artifact reduction (transverse CT slices of an example patient with hip implants) depending on MonoCT energy. *Abbreviations:* CT = computed tomography; MonoCT = pseudo-monoenergetic CT dataset; Mono = dual-energy CT application Monoenergetic imaging; MonoNIST = monoenergetic CT numbers derived from (26); MonoPlus = dual-energy CT application syngo.CT DE Monoenergetic Plus.

60%, respectively. Consequently, for the treatment planning comparison, MonoCTs were calculated with MonoPlus. For energies above 70 keV, MonoPlus provides MonoCTs with an image noise comparable with that of 120 kVp SECT. In the energy region from 75 to 80 keV, the INR can even be increased by 10%.

Mono and MonoPlus reveal a similar energy-dependent BHR. For energies between 75 and 95 keV, MonoCTs contribute to better CT number stability concerning different beam hardening conditions in comparison with 120 kVp SECT. The maximal BHR is reached at 79 keV, which leads to a reduction of beam hardening by 23% on average over all tissues and up to 69% for bones. This corresponds to a reduction of range variabilities on average from 1.0 mm to 0.8 mm and maximal from 2.7 mm to 2.2 mm for 15 cm tissue penetration, when all tabulated human tissues (excluding lung) in the 3 scan setups are considered.

Determination of MonoCT weighting factor

The determined weighting factor α (E_{mono}) for MonoCT calculation is shown in Figure 1 for Mono, MonoPlus, and MonoNIST. The energy dependence of α was fitted with a power-law function. Fit parameters are presented in Supplement EC (available online at www.redjournal.org). Mono and MonoPlus use the same energy-dependent weighting factor. Given that α is nearly 0 for MonoCTs of 79 keV, these datasets are comparable with those of 140 kVp SECT scans in image noise and beam hardening.

Pseudo-monoenergetic CT numbers obtained by Mono and MonoPlus differ from monoenergetic CT numbers (MonoNIST), which may be caused by the vendor-specific calibration of Mono and MonoPlus. For example, 120 keV pseudo-monoenergetic CT numbers correspond to 140 keV monoenergetic CT numbers because $\alpha = -0.62$ is used for MonoCT calculations in Mono and MonoPlus instead of $\alpha = -0.52$ for MonoNIST.

The evaluation of all investigated materials and scan setups reveals negligible error bars of α (E_{mono}), indicating a sufficiently accurate calculation of monoenergetic CT numbers. Even MonoCTs below the mean energy of the 80 kVp scan ($\alpha > 1$) and beyond the mean energy of the 140 kVp scan ($\alpha < 0$) can be accurately determined by compensating the different impact of X-ray interactions (incoherent scattering vs photoelectric effect).

Definition of CT-number-to-SPR conversion

In Figure 2, the Hounsfield look-up tables based on 120 kVp SECT and 79 keV MonoCT are compared. A 79 keV MonoCT is particularly suitable for treatment planning because beam hardening is less pronounced (BHR maximum) and image noise is most reduced for MonoPlus (INR maximum), as shown in Figure 1. Both HLUTs are quite similar for low-density materials and soft tissues ($H < 50$ HU) because of their major dependence on electron density. HLUT differences in the bony region are induced by the strong energy dependence of x-ray attenuation for materials with a higher effective atomic number than water. This implies a steeper slope with increasing x-ray energy, which is associated with a more sensitive response on CT number changes. In comparison with 120 kVp SECT, HLUT residuals of tabulated human tissues for 79 keV MonoCTs are slightly reduced from a root-mean-square deviation of 1.5% to 1.2%, suggesting slightly fewer differences between tissue substitutes (used for calibration) and the tabulated human tissues. Materials differing from tissue compositions, like polymers or metals, can significantly deviate from the calibration curve and are therefore in general not appropriately covered by any heuristic CT-number-to-SPR conversion.

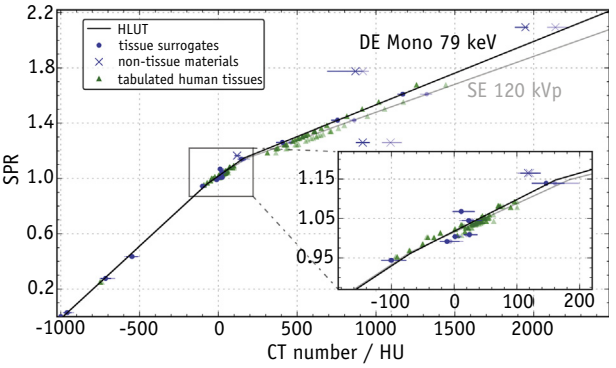

Fig. 2. CT-number-to-SPR conversion for proton treatment planning on 79 keV MonoCTs (nontransparent) and 120 kVp SECT scans with a mean energy of 64 keV (semitransparent). *Abbreviations:* CT = computed tomography; DE = dual energy; HLUT = Hounsfield look-up table; MonoCT = pseudo-monoenergetic CT dataset; SECT = single-energy CT; SPR = stopping-power ratio.

Evaluation of dose calculation

Head phantom

To quantify differences in proton range prediction between 120 kVp SECT and 79 keV MonoCT, a treatment planning comparison on a head phantom was performed. One hundred forty-six line-dose profiles in beam direction with 1 mm spacing were analyzed considering all transverse CT slices receiving the prescribed dose. In a comparison of SECT-based and MonoCT-based dose calculations, mean absolute range differences between both 0.31 ± 0.15 mm at R_{90} and 0.31 ± 0.13 mm at R_{80} were revealed. The maximal absolute range difference was 0.71 mm for R_{90} and 0.59 mm for R_{80}. All range differences were thus smaller than the used dose grid dimensions. Figure 3 shows 3 representative line-dose profiles and their range differences between 79 keV MonoCT and 120 kVp SECT.

A 2-dimensional γ analysis (1%, 1 mm) of the dose distributions resulted in a mean and minimal γ passing rate

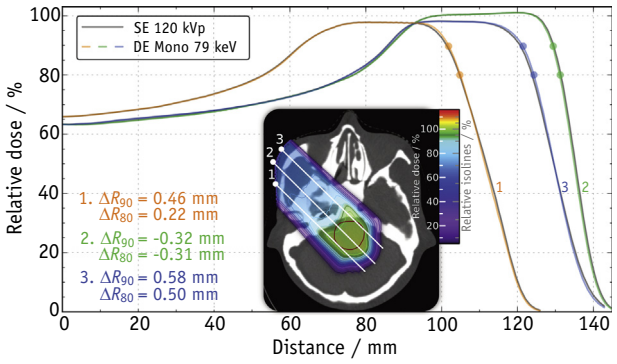

Fig. 3. Representative line-dose profiles in a head phantom to quantify potential deviations between range prediction using either 120 kVp SECT scans or DECT-based 79 keV MonoCTs. *Abbreviations:* CT = computed tomography; DECT = dual-energy CT; MonoCT = pseudo-monoenergetic CT dataset; SECT = single-energy CT.

of 99.92% and 99.60%, respectively. In summary, an excellent agreement of both dose distributions within the limits of the chosen dose grid dimensions has been proved.

Patient

The agreement between SECT-based and MonoCT-based dose calculations was confirmed in the evaluation of a clinical patient treatment plan: range deviations between SECT-based and MonoCT-based dose calculations were comparable to those determined in the head phantom and thus within dose grid dimensions, as shown in Figure 4 with 3 representative line-dose profiles. In line, the γ analysis revealed a mean and minimal γ passing rate greater than 99.99% and 99.98%, respectively. Consequently, no clinically relevant changes in the patient's dose-volume histogram can be observed.

Discussion

Given that DECT imaging can potentially reduce CT-related uncertainties in treatment planning, the clinical applicability of DECT in proton therapy was evaluated in this study. Inasmuch as DECT-based voxelwise SPR algorithms are not yet mature for clinical application, this work was focused on the use of pseudo-monoenergetic CT datasets calculated from DECT scans, still relying on a heuristic CT-number-to-SPR conversion. Nevertheless, this study could demonstrate not only safety and feasibility of this specific DECT application for proton treatment planning but also slight benefits.

After optimization of SECT and DECT for radiation therapy concerning image noise and beam hardening, it could be shown that DECT-based MonoCTs can contribute to improved image quality (ie, increased INR and BHR) in comparison with 120 kVp SECT. Owing to efficient noise reduction in the MonoPlus algorithm, the image quality of

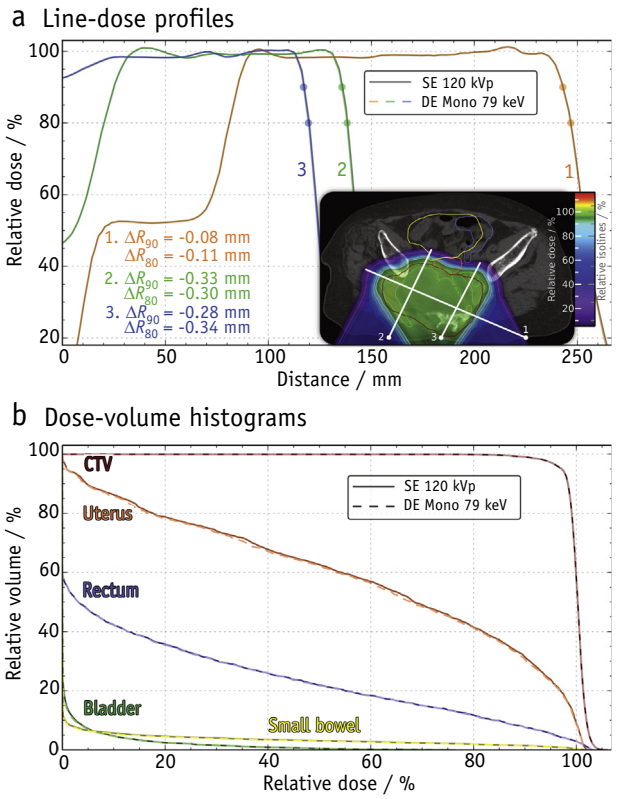

Fig. 4. Representative (a) line-dose profiles and (b) dose-volume histograms of a patient treatment plan for irradiation of a sacral chordoma calculated on both 120 kVp SECT scan and 79 keV MonoCT. *Abbreviations:* CT = computed tomography; MonoCT = pseudo-monoenergetic CT dataset; SECT = single-energy CT.

MonoCTs is considerably enhanced when the application MonoPlus is used instead of Mono. Consequently, clinical calculations of MonoCTs should be performed with MonoPlus. In general, these results (especially concerning scan protocol and image reconstruction parameters) can be directly transferred to voxelwise DECT-based SPR approaches because they are also image based.

For 80/140 kVp DECT scans, 79 keV MonoCTs reveal low image noise and the slightest beam hardening effects on CT numbers. This leads to reduced CT-related interpatient variabilities, especially between targets of different body regions or patients of different physique, which ultimately enable a slightly more reliable SPR prediction. Therefore, 79 keV MonoCTs (corresponding to 83 keV MonoNIST) were chosen for proton treatment planning.

Based on a patient's DECT scan, more than one MonoCT dataset optimized for proton treatment planning can be generated. Various MonoCTs with different energies can be calculated to offer clinicians more possibilities for delineating, for example, low-energy MonoCTs for better contrast-to-noise ratio and high-energy MonoCTs for metal artifact reduction (13, 19), as exemplarily, shown in Figure 1 for a patient with hip implants. The question whether these additional opportunities can lead to a

reduction of delineation uncertainties still has to be shown in clinical studies. So far, studies have mostly focused only on improving image quality (14-18).

In addition to the enhanced image quality of MonoCTs in comparison with 120 kVp SECT, the heuristic CT-number-to-SPR conversion is also slightly more precise when 79 keV MonoCT is used. Further improvements relate to the CT number prediction of tabulated human tissues, which are commonly used for HLUT definition. For SECT, the CT numbers of these materials are determined by a scanner-specific stoichiometric CT number prediction. But for MonoCTs they can be calculated more simply by the use of tabulated monoenergetic material-specific photon cross-sections (26) multiplied with the scanner-specific weighting-factor ratio $\widehat{\alpha} = \alpha_{\mathrm{MonoPlus}}(E_{\mathrm{mono}})/\alpha_{\mathrm{MonoNIST}}(E_{\mathrm{mono}})$.

As shown in a head phantom and especially in a clinical patient case, SECT-based and MonoCT-based heuristic proton range predictions and dose distributions are consistent. The benefits concerning interpatient variabilities of SPR prediction, which have been shown in the evaluation of different beam hardening conditions, could by definition not be reconfirmed in this single case study.

In consideration of all results achieved within this study, proton treatment planning based on MonoCTs was clinically implemented at the University Proton Therapy Dresden (UPTD) in 2015 to reduce CT-related uncertainties caused by beam hardening and to make use of additional DECT options for delineating. According to our information, UPTD is the first proton therapy center performing treatment planning on the basis of DECT scans. Until October 2016, more than 950 DECT scans of overall 351 patients were acquired with the use of standardized, and for radiation therapy optimized scan protocols. This continuously growing DECT patient database offers the unique opportunity to validate voxelwise SPR prediction methods (8, 12) on many patient datasets to perform analyses of intrapatient and interpatient variability, to test the robustness of several SPR approaches, to realistically quantify the possible benefit of DECT, and consequently to estimate the potential range uncertainty reduction resulting in smaller therapeutic margins.

It must be emphasized that only one patient case could be included because both a SECT and a DECT scan can be justified only in very rare cases according to the ALARA principle. Therefore, a detailed and reliable range evaluation had to be performed on a head phantom and then verified for an example patient case, which is considered sufficient to exclude possible differences of proton range predictions in phantoms and patients.

Furthermore, the comparison between SECT and DECT was based on the assumption that the total CT doses would be similar. One could argue that an improvement in treatment planning precision would justify an increased CT dose. However, every other dose specification would be more arbitrary than that chosen here.

Because 2 single DECT scans are acquired sequentially with a single-source CT scanner, the obtained images can be influenced by patient motion (eg, breathing, swallowing, or organ movements) occurring within the timespan of acquisition. Consequently, treatment planning based on DECT was initially implemented for tumor entities and body regions, where patient motion can be neglected between both CT scans (eg, brain and skull target sites-more than 50% of all patients). On the basis of control CT scans, which are acquired in dual-energy mode for all patients during proton treatment, the impact of motion on sequential DECT scans is analyzed to possibly widen the spectrum of tumor entities scanned in dual-energy mode for treatment planning (eg, for targets in the pelvic region).

In conclusion, this study demonstrates that DECT-based treatment planning using MonoCTs is feasible and safe. Furthermore, it leads to decreased image noise and beam hardening in comparison with 120 kVp SECT with the same CT dose and enables more opportunities for defining clinical contours. This already contributes to a slightly more reliable proton range prediction. On the basis of these results, proton treatment planning using MonoCTs was clinically implemented. Further improvements are expected from a physics-based, patient-specific, nonheuristic SPR determination. The continuously growing clinical database of standardized DECT scans offers unique opportunities for evaluating different DECT-based SPR prediction approaches and for quantifying intrapatient and interpatient tissue variabilities.

References

1. van de Water TA, Bijl HP, Schilstra C, et al. The potential benefit of radiotherapy with protons in head and neck cancer with respect to normal tissue sparing: A systematic review of literature. *Oncologist* 2011;16:366-377.
2. Nichols RC, Huh SN, Prado KL, et al. Protons offer reduced normal-tissue exposure for patients receiving postoperative radiotherapy for resected pancreatic head cancer. *Int J Radiat Oncol Biol Phys* 2012;83:158-163.
3. Jakobi A, Bandurska-Luque A, Stützer K, et al. Identification of patient benefit from proton therapy for advanced head and neck cancer patients based on individual and subgroup normal tissue complication probability analysis. *Int J Radiat Oncol Biol Phys* 2015;92:1165-1174.
4. Paganetti H. Range uncertainties in proton therapy and the role of Monte Carlo simulations. *Phys Med Biol* 2012;57:R99-R117.
5. Knopf A-C, Lomax AJ. In vivo proton range verification: A review. *Phys Med Biol* 2013;58:R131-R160.
6. Yang M, Virshup G, Clayton J, et al. Theoretical variance analysis of single- and dual-energy computed tomography methods for calculating proton stopping power ratios of biological tissues. *Phys Med Biol* 2010;55:1343-1362.
7. Saito M. Potential of dual-energy subtraction for converting CT numbers to electron density based on a single linear relationship. *Med Phys* 2012;39:2021-2030.
8. Hünemohr N, Krauss B, Tremmel C, et al. Experimental verification of ion stopping power prediction from dual energy CT data in tissue surrogates. *Phys Med Biol* 2014;59:83-96.
9. Hünemohr N, Paganetti H, Greilich S, et al. Tissue decomposition from dual energy CT data for MC based dose calculation in particle therapy. *Med Phys* 2014;41:61714.

10. Tsukihara M, Noto Y, Sasamoto R, et al. Initial implementation of the conversion from the energy-subtracted CT number to electron density in tissue inhomogeneity corrections: An anthropomorphic phantom study of radiotherapy treatment planning. *Med Phys* 2015;42:1378-1388.
11. Hudobivnik N, Schwarz F, Johnson T, et al. Comparison of proton therapy treatment planning for head tumors with a pencil beam algorithm on dual and single energy CT images. *Med Phys* 2016;43:495-504.
12. Möhler C, Wohlfahrt P, Richter C, et al. Range prediction for tissue mixtures based on dual-energy CT. *Phys Med Biol* 2016;61:N268-N275.
13. Kuchenbecker S, Faby S, Sawall S, et al. Dual energy CT: How well can pseudo-monochromatic imaging reduce metal artifacts? *Med Phys* 2015;42:1023-1036.
14. Grant KL, Flohr TG, Krauss B, et al. Assessment of an advanced image-based technique to calculate virtual monoenergetic computed tomographic images from a dual-energy examination to improve contrast-to-noise ratio in examinations using iodinated contrast media. *Invest Radiol* 2014;49:586-592.
15. Wichmann JL, Nöske E-M, Kraft J, et al. Virtual monoenergetic dual-energy computed tomography: Optimization of kiloelectron volt settings in head and neck cancer. *Invest Radiol* 2014;49:735-741.
16. Forghani R, Levental M, Gupta R, et al. Different spectral Hounsfield unit curve and high-energy virtual monochromatic image characteristics of squamous cell carcinoma compared with nonossified thyroid cartilage. *AJRN Am J Neuroradiol* 2015;36:1194-1200.
17. Husarik DB, Gordic S, Desbiolles L, et al. Advanced virtual monoenergetic computed tomography of hyperattenuating and hypoattenuating liver lesions. *Invest Radiol* 2015;50:695-702.
18. Kaup M, Scholtz J-E, Engler A, et al. Dual-energy computed tomography virtual monoenergetic imaging of lung cancer: Assessment of optimal energy levels. *J Comput Assist Tomogr* 2016;40:80-85.
19. Mangold S, Gatidis S, Luz O, et al. Single-source dual-energy computed tomography: Use of monoenergetic extrapolation for a reduction of metal artifacts. *Invest Radiol* 2014;49:788-793.
20. Woodard HQ, White DR. The composition of body tissues. *Br J Radiol* 1986;59:1209-1219.
21. White DR, Woodard HQ, Hammond SM. Average soft-tissue and bone models for use in radiation dosimetry. *Br J Radiol* 1987;60:907-913.
22. Schneider U, Pedroni E, Lomax AJ. The calibration of CT Hounsfield units for radiotherapy treatment planning. *Phys Med Biol* 1996;41:111-124.
23. Schneider W, Bortfeld T, Schlegel W. Correlation between CT numbers and tissue parameters needed for Monte Carlo simulations of clinical dose distributions. *Phys Med Biol* 2000;45:459-478.
24. Schabel C, Bongers M, Sedlmair M, et al. Assessment of the hepatic veins in poor contrast conditions using dual energy CT: Evaluation of a novel monoenergetic extrapolation software algorithm. *Rofo* 2014;186:591-597.
25. Albrecht MH, Scholtz J-E, Kraft J, et al. Assessment of an advanced monoenergetic reconstruction technique in dual-energy computed tomography of head and neck cancer. *Eur Radiol* 2015;25:2493-2501.
26. Berger MJ, Hubbell JH, Seltzer SM, et al. XCOM: Photon Cross Section Database (online version 1.5, 2010). *NIST Standard Reference Database 8* 1990; available: http://physics.nist.gov.xcom.
27. Jäkel O, Jacob C, Schardt D, et al. Relation between carbon ion ranges and x-ray CT numbers. *Med Phys* 2001;28:701-703.
28. Seltzer SM, Berger MJ. Evaluation of the collision stopping power of elements and compounds for electrons and positrons. *Int J Appl Radiat Isot* 1982;33:1189-1218.
29. Bragg WH, Kleeman R. On the alpha particles of radium, and their loss of range in passing through various atoms and molecules. *Philos Mag* 1905;10:318-340.
30. Low DA, Harms WB, Mutic S, et al. A technique for the quantitative evaluation of dose distributions. *Med Phys* 1998;25:656-661.